Influence of high-energy ball milling on structural, microstructural, and optical properties of Mg_2TiO_4 nanoparticles

Ranjan Kumar Bhuyan[1,2] · Ranjan Kumar Mohapatra[3] · Ganeswar Nath[4] · Basanta Kumar Sahoo[2] · Debadutta Das[5] · D. Pamu[1]

Abstract

In this paper, we report the impact of mechanical activation on structural, microstructural, thermal, and optical properties of Mg_2TiO_4 (MTO) nanoparticles prepared by high-energy ball milling. Williamson–Hall (W–H) method was carried out in order to understand the origin of the broadening in the X-ray diffraction (XRD) peaks and for the estimation of crystallite size of MTO nanocrystalline powder. It is revealed that the peak broadening is not only due to reduced coherently diffracting domain size but also due to a significant strain distribution. The calculated strain was 9.0×10^{-3} and the average crystallite sizes are 40–60 nm for 35-h milled powder and this result is consistent with transmission electron microscopy (TEM) analysis. To examine the nature of lattice fringes for the 35-h milled samples, high-resolution TEM study was carried out. It revealed that the as-prepared samples are highly crystalline in nature. The surface morphological studies were carried out by using scanning electron microscopy (SEM) and atomic force microscopy (AFM). Further, MTO nanoparticles showed a strong absorption at ~356 nm, and the bandgap values ranged between 3.26 and 3.78 eV with an increase of milling time from 0 to 35 h. The photoluminescence (PL) spectrum measured at room temperature showed the bands which are belong to the near band edge emission at 357 nm. The MTO nanoparticles prepared by mechanical alloying method exhibited promising optical properties which are suitable for commercial optoelectronic applications.

1 Introduction

The growing importance of ceramics has lead to great advances in the material research and development of dielectric systems for various applications such as microwave oscillators, amplifiers, filters, etc. [1–4]. Recently, the demand of low-loss dielectric materials in different fields

✉ Ranjan Kumar Bhuyan
   ranjanphysics.bhuyan8@gmail.com

✉ Ranjan Kumar Mohapatra
   ranjank_mohapatra@yahoo.com

1 Department of Physics, Indian Institute of Technology Guwahati, Guwahati 39, India

2 Department of Physics, Govt. (Auto) College, Angul, Odisha 143, India

3 Department of Chemistry, Government College of Engineering, Keonjhor, Odisha 758002, India

4 Department of Physics, Veer Surendra Sai University of Technology, Burla, Sambalpur, Odisha 18, India

5 Department of Chemistry, Sukanti Degree College, Subarnapur, Odisha 767017, India

has been increased [3–5]. Moreover, the dielectrics having low permittivity play an importance role to minimize cross coupling with conductors and to reduce time for the electronic signal transition. However, due to rise in carrier frequency, the materials having high-quality factor ($Q \times f_o$) and nearly zero temperature coefficient of resonant frequency (τ_f) (which needs to counter the stability of the frequency against the change in temperature) are most essential. There are huge numbers of microwave dielectrics proposed to satisfy this requirement for high-frequency applications [5–12], due to which, high Q dielectric materials such as MgO–TiO_2 binary system have brought much more attention. There are basically three stable phases ($MgTiO_3$, Mg_2TiO_4, and $MgTi_2O_5$) in the MgO–TiO_2 system reported [13, 14]. Out of them, Mg_2TiO_4 ceramic is one of the best microwave dielectric ceramics, with excellent dielectric properties: high-quality factor ($Q \times f_o$) ~ 150,000 GHz, average dielectric constant (ε_r) ~ 14, and a negative temperature coefficient of resonant frequency (τ_f) ~ −50 ppm/°C [11, 13, 14].

Now-a-days, importance of nanomaterials has been increased in different fields. This is due to their distinct physical and chemical properties which are significantly

different from bulk counterparts [15]. In this study, MTO nano-ceramics were synthesized by high-energy ball milling process, which is an economical, more-suited, and well-regulated method for the synthesis of any class of nanosized metallic and ceramic powders [16, 17]. The most significant advantage of this method is that the solid-state reaction is initiated via mechanical energy without producing heat energy. Moreover, the samples synthesized by this method possess higher sinterability as compared to those synthesized from solid-state reaction and most of the wet chemical methods [18]. The method has many advantages: it makes the material finer, helps to find out structural changes developed in the material, phase transformations, and even solid-state reactions among the solid reagents. These physicochemical changes take place due to intensive mechanical force during the milling process which causes transformation of the mechanical energy to the grinding particles [19].

In view of the above advantages, MTO nano-powders have been prepared with the help of high-energy ball mill and intend to investigate its effect on crystal structure, microstructure, and optical properties as well as on thermodynamics of MgO–TiO_2 system.

2 Experimental details

2.1 Processing

Pure Mg_2TiO_4 powders were prepared via high-energy ball milling method from high-purity oxides MgO (99.9%) and TiO_2 (99.9%) of Sigma-Aldrich (St. Louis, MO). The initial powders MgO and TiO_2 were mixed in required stoichiometry ratio and the mixture was ball milled (using planetary ball mill (Fritsch GmbH, Germany)) for different hours up to steady-state condition. During ball milling, the following conditions are maintained: (i) ball-to-powder ratio: 10:1; ball diameter: 8 and 16 mm; ball and vial materials: tungsten carbide; speed: 350 rpm. After a regular interval of time (30 min), the milling was stopped and then resumed for 5 min, to avoid significant temperature rise.

2.2 Characterizations

Room temperature X-ray diffraction (XRD) (Rigaku TTRAX 18 KW) with Cu-K_α radiation was employed to determine the phase structures of the different hours of milled MTO powder. The thermal decomposition response of the different hours of milled powders was studied by a thermogravimetric analyzer (TGA STA 449-F3, NETZSCH, Jupiter) in the argon atmosphere at a heating rate of 10 °C/min. Transmission electron microscope (TEM) (JEOL-JEM-2100) was used to identify nanosized particle images of different hours of milled powders. Scanning electron microscopy

(LEO 1430-VP) was used to analyze morphology of the MTO powder particles. Further, scanning probe microscope (Seiko Instruments Inc., SPA-400) was employed in the contact atomic force microscopy (AFM) mode to characterize the surface morphology of the MTO powders. UV–VIS–NIR spectrophotometer (UV 3101PC, Shimdzu) was used to obtained UV/VIS absorption spectra of all the samples in the wavelength range 200–1000 nm. Room temperature photoluminescence (PL) measurement was carried out by using thermo-spectronic (Aminco-Bowman-2) double monochromator coupled to a GaAs photomultiplier with a conventional photon counting system.

3 Results and discussion

3.1 Structural analysis

To monitor the influence of high-energy ball milling on the initial powders, XRD patterns were recorded for the powders milled for different hours. The X-ray powder diffraction patterns of MgO–TiO_2 systems milled for 5, 20, 30, and 35 h are illustrated in Fig. 1. It was noticed that the MTO powder milled for 5 h exhibited the peaks corresponding to parent compounds only, such as MgO and TiO_2. With increases of milling time, the intensities of the parent oxide peaks depressed gradually and the formation of $MgTi_2O_5$ phase was observed. When the milling time reached at 30 h, all the parent oxide peaks disappeared completely resulting in high-intense diffraction peak of pure MTO phase with small significance of $MgTiO_3$ and $MgTi_2O_5$ phases. However, at 35-h milling, the sample showed more intensified MTO phases along with small $MgTiO_3$ phase, which suggests
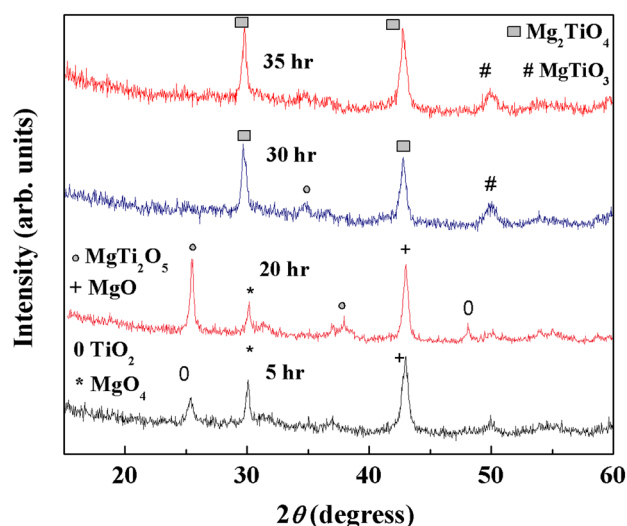

Fig. 1 XRD patterns of the MgO and TiO_2 oxides milled for 5, 20, 30, and 35 h

that crystallite nature of pure MTO sample enhances. The presence of diverse phases such as $MgTi_2O_5$ and $MgTiO_3$ in the $MgO–TiO_2$ system is mostly due to the difference in the degree of the incipient mechanical reaction. This can be illustrated as follows: during the process of mechanical alloying, the mechanical energy of the grinding media transforms into the parent oxide particles which causes structural destruction followed by reduction in particle size [19].

The crystallite size of nanoparticles can be determined with several techniques that rely upon the peak width of the X-ray diffraction patterns. In the present study, Williamson–Hall (W–H) plot method as well as Scherrer formula have been chosen in order to understand the origin of the broadening in the XRD peaks.

3.1.1 Structural analysis based on Williamson–Hall method

According to W–H method [20], the peak broadening due to lattice strain can be calculated using the following formula:

$$\beta \cos\theta = \left[\frac{k\lambda}{D_{WH}}\right] + 4e\sin\theta, \quad (1)$$

where β is full width at half maximum (FWHM) of the Bragg peaks (in radians), θ is Bragg's angle of the analyzed peaks, λ is wavelength of the X-ray (here, λ is 0.154056 nm for Cu-K$_\alpha$), D_{WH} is average crystallite size, and e is effective strain associated with mechanical alloying.

Further, the broadening due to small crystallite size may be expressed by using Debye–Scherrer's equation, i.e.,

$$\beta_c = \frac{k\lambda}{D\cos\theta}, \quad (2)$$

where β_c is the full width half maximum, D is the crystallite size, k is the shape factor ($=0.9$ for spherical particles), and λ is the wavelength of Cu-K$_\alpha$ radiation.

The variation of average crystallite size as a function of milling time was estimated from Eqs. (1 and 2) and represented in Fig. 2a. It found that up to 30 h of milling, the average crystallite size decreases rapidly and beyond which it attained a constant value. The as-mixed powders have an average crystallite size of nearly 2.5 μm. After milling of 20 h, the crystallite size reduced to 100–120 nm and further to 40–60 nm for 35 h of milling. But, using Scherrer formula, the average crystallite sizes for MTO powder after 20 and 35 h of milling are found to be 28 nm and 17 nm, respectively. Thus, the crystallite size obtained using Scherrer's equation is smaller than the W–H method. The difference is mainly due to the fact that the Scherrer's equation does not account for lattice strain effect on the peak broadening. The inset of Fig. 2a illustrates the variation of lattice parameter with milling time. It reveals that with an increase of milling time, the lattice constant decreases from 8.436 Å to nearly a stable value of 8.412 Å, beyond 35 h of milling. The variation in lattice constant indicates the happening of atomic disorder during the milling process. The mechanical alloying process not only reduces the crystallite size into nanometric size but also causes an enhancement in the lattice strain. The total broadening of the XRD peaks is mostly caused due to the reduction of crystallite size, lattice strain, and the instrumental effects. Crystallite size is a measure of the size
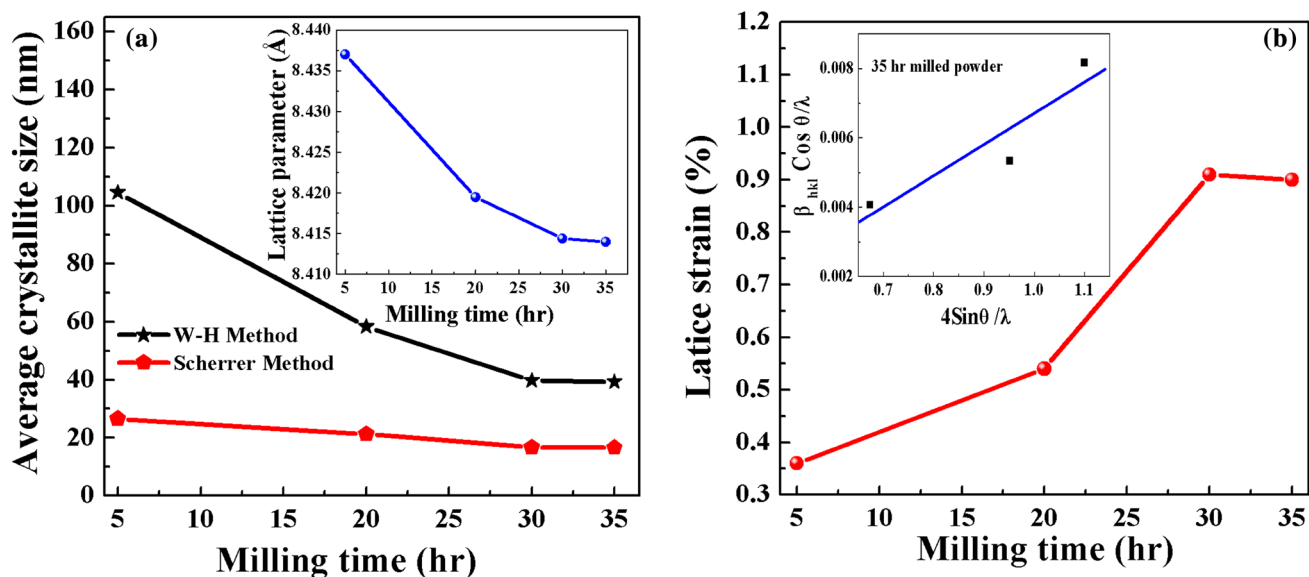

Fig. 2 a Variations of average crystallite size and lattice parameter (inset) with milling time and **b** variation of lattice strain with milling time. Inset: W–H plot for 35-h milled powders

of a coherently diffracting domain. When the crystallites of the materials are very small (< 100 nm), they have less number of parallel diffraction planes producing broadened diffraction peaks. Likewise, the non-uniform strains arising out of heavy plastic deformation during mechanical alloying process cause broadening of the diffraction peaks. The other sources of strain are the grain boundary triple junctions, crystal imperfections, etc. [19].

The milling dependence of internal microstrain (e) of mechanically alloyed MTO powders was calculated and depicted in Fig. 2b. Figure 2b (inset) shows the plot (known as W–H plots) between $4\sin\theta/\lambda$ and $\beta_{hkl}\cos\theta/\lambda$ for selected diffraction peaks for 35-h milled MTO nano-powders. The deviation in the data points from the straight line suggests that the strain is anisotropic. The average crystallite was estimated from the y-intercept as 38 nm and the strain (e) from the slope of the linear fit as 9.0×10^{-3}, for 35-h milled powders. From the W–H analysis, it is clearly seen that the broadening of the peaks in XRD is due to the contribution of small crystallite size and the anisotropic strain. It was also

observed that the internal strain enhanced with an increase in milling time and subsequently attains the saturated value.

3.2 Morphological study on mechanically alloyed MTO powders

3.2.1 SEM analysis

SEM micrographs generally confirm the shape and size of the as-prepared samples. To see the influence of mechanical activation on the evolution of microstructure of MTO powders, SEM micrographs were obtained. Figure 3 shows the SEM micrographs of the as-mixed as well as milled powders. It is very well known that during mechanical destruction by high-energy ball milling, the development of materials phases is coupled to the mechanical properties of the powders and thus to their microstructures [21, 22]. Generally, the evolution of microstructure is restricted by milling strength, the temperature, and the composition of the materials.
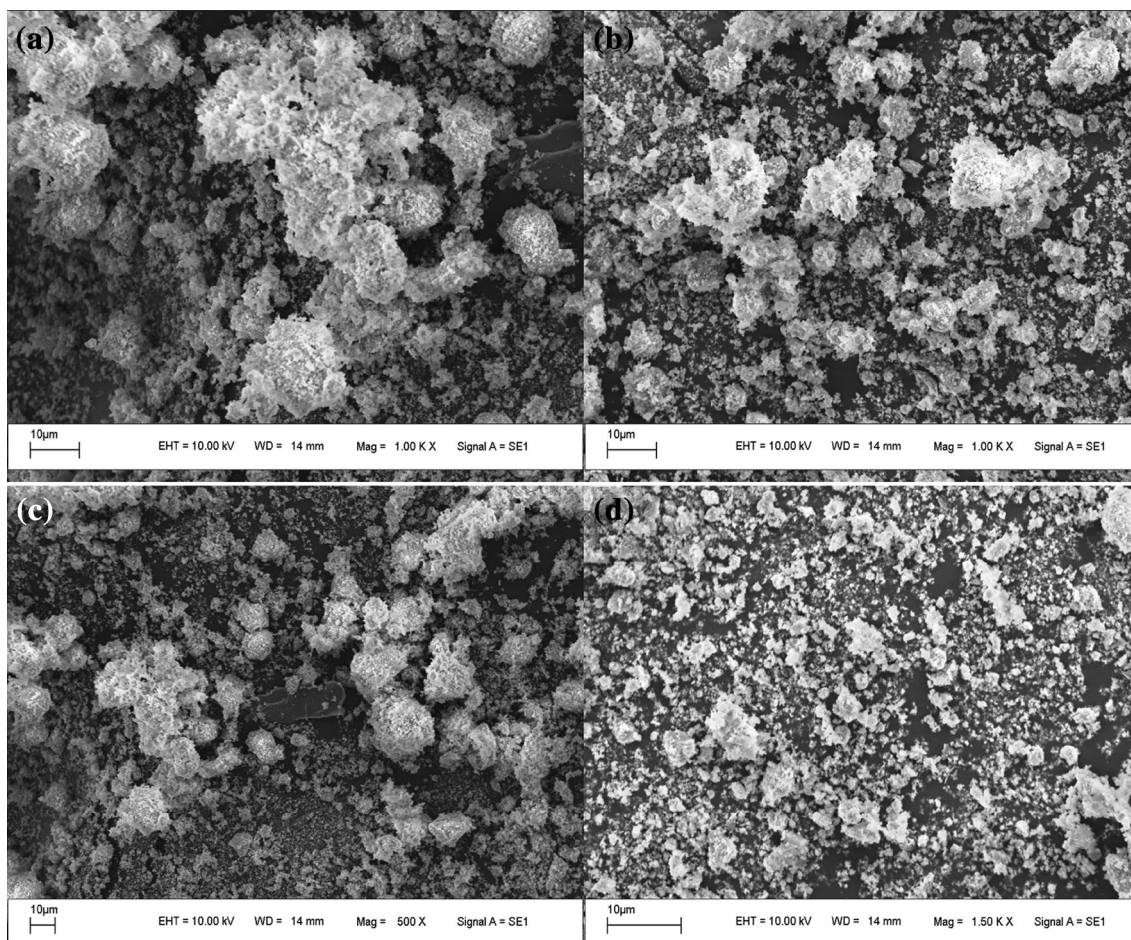

Fig. 3 SEM micrographs of the MTO powders milled for **a** 0, **b** 5, **c** 20, and **d** 35 h

From the microstructural analysis, it is observed that the initial as-mixed powders (Fig. 3a) consist of nearly spherical particles with agglomerated morphology. After 5 h of milling, the particle morphology is found to be spherical (Fig. 3b) but the particle size was varied from sub-micrometer to few micrometers. With increase of further milling time, the particle size reduces into nanometer range with more distinct grains compared to early stages of milling. Also, the presence of new phases was found in the shape of agglomerates covered with many nanosized particles of starting powders. These agglomerations are characteristics of mechanically derived powders which are the outcomes of repeated cold welding and fracture of powder during high-energy ball milling. The SEM results give the support as evidence to the XRD results and showed that

the crystalline nature of the MTO sample enhances with the increase in milling time.

3.2.2 AFM analysis

To observe the influence of milling time on the topography of the MTO nanoparticles, AFM analysis is performed. Figure 4 shows the typical AFM images of the MTO nanoparticles obtained after milling time of 20 and 35 h, respectively. Using AFM analysis, the average size of the MTO nanoparticles is found to be 80–120 nm for 20 h of milling and 40–80 nm for 35 h milling. The root-mean-square (rms) roughness varied from 4.46 to 7.63 nm as the milling time increases from 20 to 35 h. AFM micrographs indicate that the particles have an inhomogeneous nature with no granular structure for 20-h milled powders. This could be
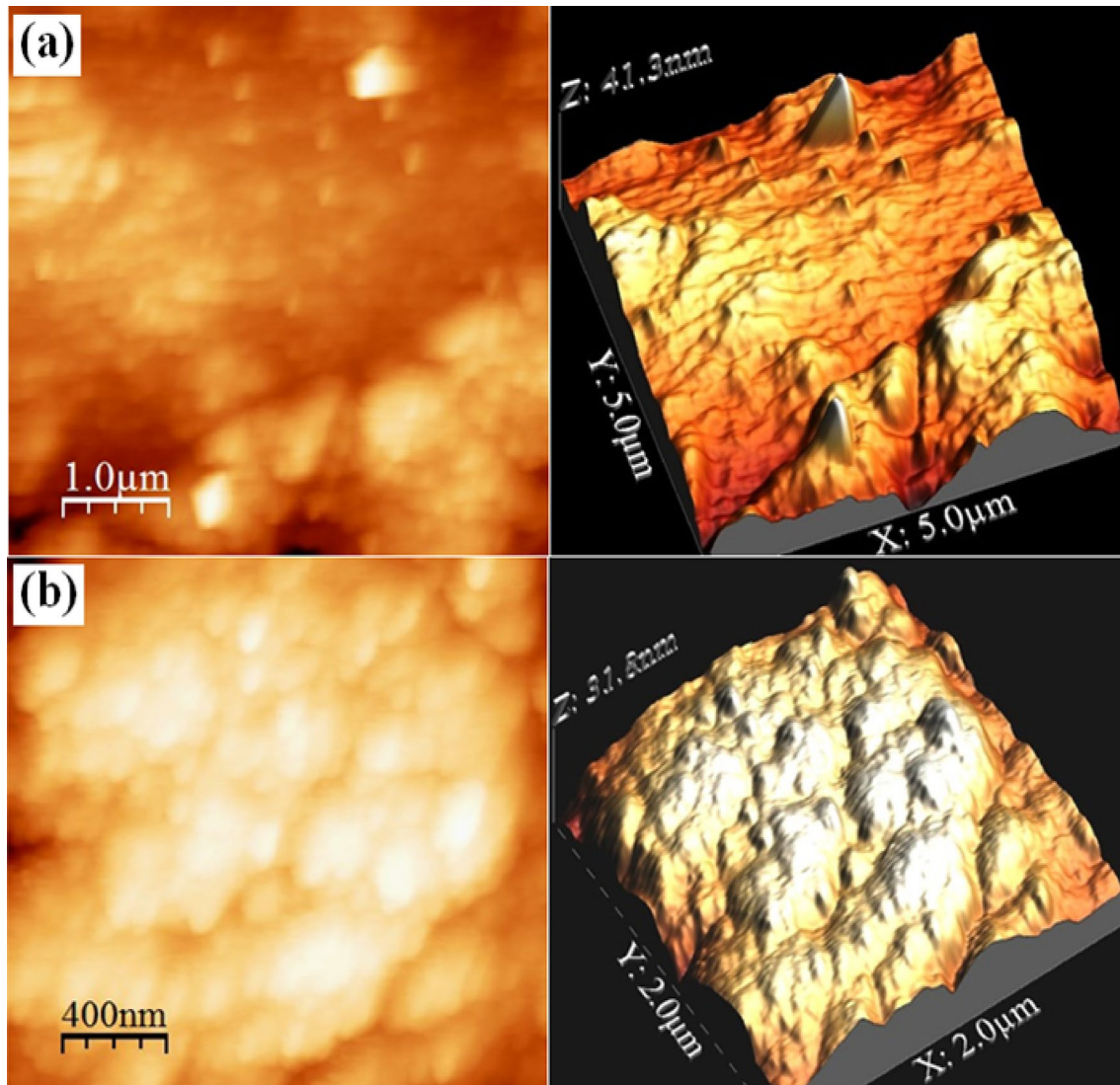

Fig. 4 AFM topography of MTO powders milled for **a** 20 and **b** 35 h

attributed to the structural disorder in the long and short range as revealed by the XRD analysis. The surface morphology of MTO powders milled for 35 h shows the characteristics of nanoparticles of an order (crystalline) material. The AFM result is consistent with the microstructure obtained using SEM. Both SEM and AFM analysis of the MTO nanoparticles showed that the shapes of the nanoparticles are spherical.

3.2.3 TEM analysis

The transmission electron microscopy (TEM) is a very powerful tool widely used in material science. The advantage of this technique is that it gives detail information of internal structure of individual atoms. Figure 5a, b shows the bright-field TEM micrographs of MTO powders milled for 20 and 35 h. It is found that the 20-h milled powder does not have clear particle size, whereas the 35-h milled powder shows distinct particles in nanosized. The particle size of the parent oxides is about 2 μm. With the increase of milling time, the initial particle sizes reduces and for 35-h milled powder, the average particle size is found to be around 60–100 nm. This crystallite size is nearly consistent with the calculated data by Williamson–Hall plot method. The selected area electron diffraction (SAED) pattern of the 35-h milled powder is shown in Fig. 5c. The ring pattern corresponds to different d-spacing (interplanar spacing) of the pure MTO phase, which suggests
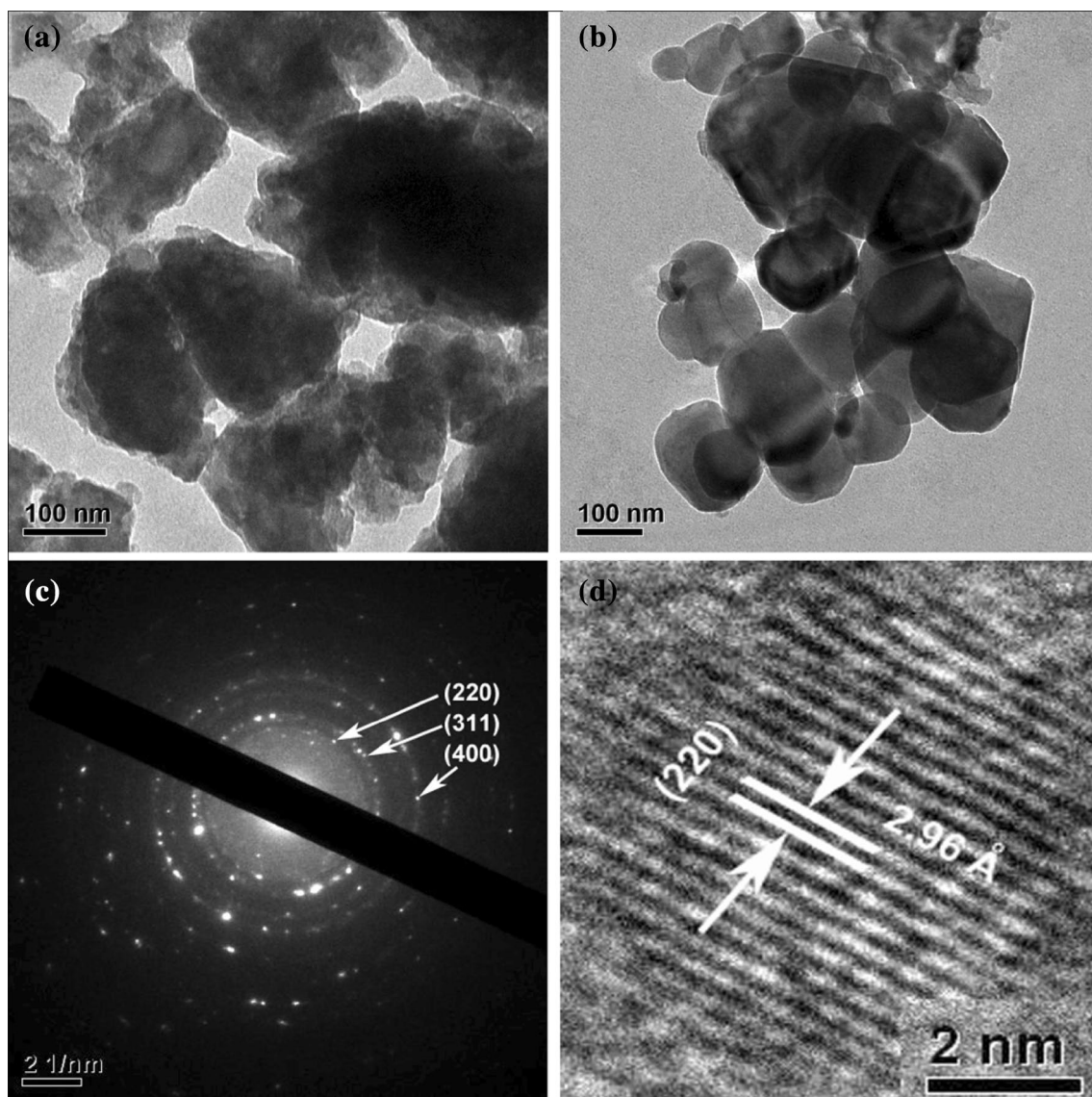

Fig. 5 Bright-field TEM micrographs of **a** 20- and **b** 35-h milled MTO powder, **c** the selected area electron diffraction (SAED) pattern, and **d** HR-TEM for 35-h milled powder

the crystalline nature of the as-prepared samples. High-resolution TEM (HR-TEM) study is carried out to evaluate the lattice fringes for the 35-h milled samples, as shown in Fig. 5d. The *d*-spacing of the crystal plane is calculated as 2.968 Å for 35-h milled powders, which indicates the preferable crystal growth plane is (220), which corresponds to the highest intensity peak in the XRD pattern of the 35-h milled powders [11]. Therefore, it can be concluded that a solid-state reaction between MgO and TiO_2 took place during the ball milling process.
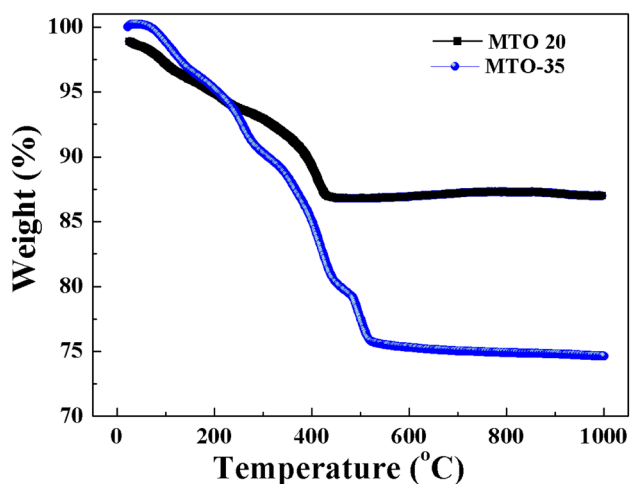

Fig. 6 Weight loss verses temperature curves for 20- and 35-h milled MTO powder

3.3 Thermal analysis

Figure 6 shows the weight loss of MgO–TiO_2 system milled for 20 and 35 h during heating. As the milling time increases, the reaction takes place at a lesser temperature in comparison with de-activated samples. As a result, the reactivity of ceramic powder improves and accelerates solid-state reactions with an increase in milling time. It is observed that the weight loss is about 5–7% up to 100 °C, which is attributed to the evaporation of water. Mechanical activation supports hygroscopic. Therefore, the weight loss is maximum for the sample with longest period of milling. So, in the present case, the powders milled for 35 h have more weight loss compared to 20-h milled powders. Further, the weight loss around 350–400 °C is more prominent due to the formation of secondary phases ($MgTiO_3$ and $MgTi_2O_5$) for both the systems. The formation of secondary phases was also confirmed by the XRD results.

3.4 Optical studies of mechanically alloyed MTO powders

To see the influence of milling time on the optical bandgap of the mechanically alloyed MTO nanoparticles, room temperature UV–visible spectra were taken for all the as-prepared samples and are shown in Fig. 7a. It is found that there is strong absorption at around 356 nm for un-milled MTO powders. With a rise in milling time, the peak slightly shifted to 352 nm for 35-h milled powders. There is a clear sign of blue-shift in the absorption peak with decrease in average crystallite size of the as-grown samples. This
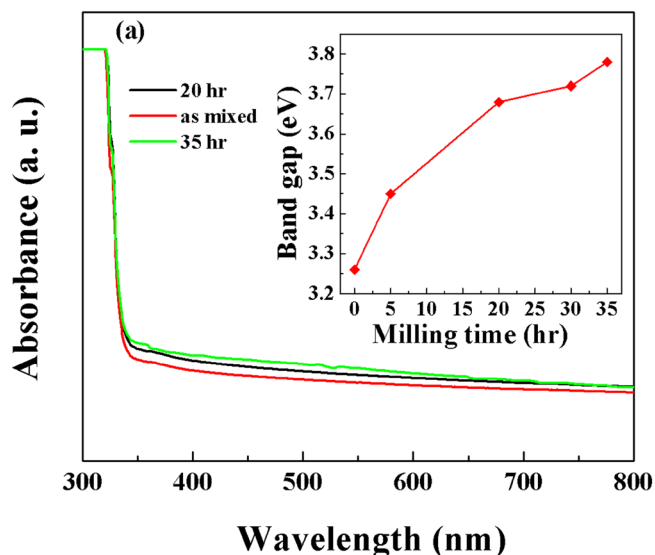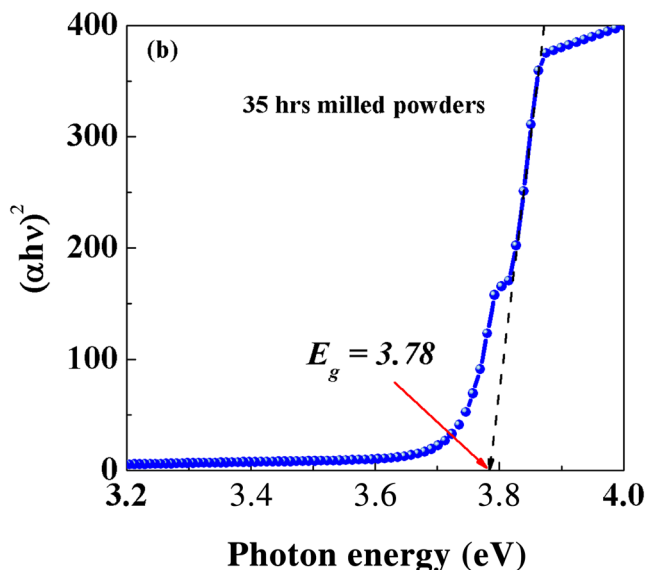

Fig. 7 **a** Room temperature UV–visible spectra of pure and milled MTO powders, INSET: variation of bandgap with milling time, and **b** variation of $(\alpha h\nu)^2$ versus photon energy for the 35-h milled powders

indicates the increase in bandgap with reduction in particle size. However, the improved absorption in nanoparticles can be attributed to a large surface-to-volume ratio and increased oscillator strength with reduction in particle size.

Tauc relation [25] is used to determine the optical bandgap of all the samples. The relation is given as, $\alpha h\upsilon = \beta (h\upsilon - E_g)^n$, where, $h\upsilon$ is the photon energy, β is a constant which measures the crystalline order of the samples, and $n = 0.5$ for direct bandgap structure (since MTO belongs to inverse spinel structures which exhibits direct bandgap). The variation of bandgap with milling time is plotted and shown in the inset of Fig. 7a. The optical bandgap (E_g) is determined by the extrapolation of the best linear fit between $(\alpha h\upsilon)^2$ and $h\upsilon$ to intercept the $h\upsilon$ axis ($\alpha = 0$), as shown in Fig. 7b. The plot indicates that the bandgap enhanced from 3.26–3.78 eV with increasing milling time from 0 to 35 h. This is comparable with the previously reported results [23–25]. Figure 7b shows the dependence of the absorption coefficients $(\alpha h\upsilon)^2$ with photon energy for the 35-h milled powders. The position and slope of the optical absorption edge make this material a suitable UV light absorber.

3.4.1 Photoluminescence analysis

Photoluminescence (PL) is the spontaneous emission of light from a material under optical excitation. Figure 8 illustrates the room temperature PL spectra of the as-milled samples. It is observed that with an increase in milling time, the broadening increases and there is only one characteristic peak at 357 nm for all the milled powders which corresponds to the near shortest visible blue-emission. The PL spectra
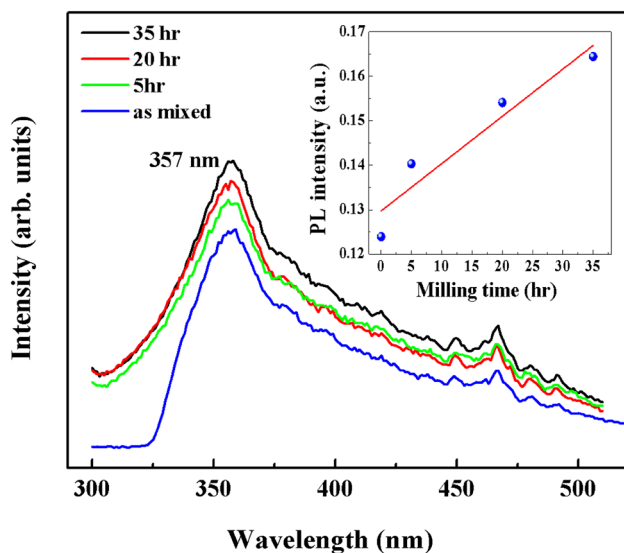
also indicate that the MTO powders milled for 35 h exhibit highest intensity with a characteristic peak at 357 nm without any significance of peak shifting. These emissions are found to be extremely broad and may be due to phonon-assisted transition and large surface-to-volume ratio of the nanosized powder.

In addition, the PL results compliment with the optical bandgap values that the increase in milling time results in the highest intensity of the peaks, which can be attributed to the high degree of structural order and disorder in the lattice [26]. Recently, a broad UV–blue PL emission with characteristic peaks around 357 and 409 nm is observed in the sputtered MTO thin films [27], which ultimately support the bulk (nano-powders) counterpart. The inset of Fig. 8 shows the variation of PL intensity with milling time. It is observed that the PL intensity increases with increasing milling time which can be attributed to a large surface-to-volume ratio of the MTO nanoparticles and increases oscillator strength with size reduction.

4 Conclusions

The influence of mechanical alloying on structural, microstructural, and optical properties of nanocrystalline MTO powders were investigated systematically. The influence of milling time on particle size, crystal structure, and the microstructure was studied using XRD, SEM, and HR-TEM analysis, respectively. Williamson–Hall method was carried out to understand the origin of the broadening of the XRD peaks and confirmed that the W–H method is a more accurate method (than Scherrer equation) for the estimation of crystallite size of the nanocrystalline powder. The microstructural analysis reveals the nanocrystalline nature of MTO ceramics prepared by mechanical alloying method. The thermal decomposition behavior of the milled powders was examined by a thermogravimetric analyzer (TGA) in argon atmosphere. The UV–visible spectra of these nanoparticles showed strong bandgap absorption at ~356 nm and an increase of the bandgap from 3.68 to 3.78 eV with an increase of milling times from 0 to 35 h. Room temperature photoluminescence spectrum of the prepared MTO nanoparticles showed band, and belongs to the near-band-edge emission at 357 nm. The Mg_2TiO_4 nanoparticles prepared by mechanical alloying method showed promising optical properties which is suitable for commercial optoelectronic applications. Also, the high optical absorption edge makes this material a suitable UV light absorber. Moreover, Mg_2TiO_4 is an excellent microwave dielectric material having wide bandgap and high refractive index and practically useful for optical and electronic applications in the form of optical modulation, infrared optical sensors, planar wave guides, electro-optic switches, etc.

Fig. 8 Room temperature photoluminescence spectrum of pure and milled MTO powders. Inset: variation of PL intensity versus milling time

References

1. R.K. Bhuyan, T.S. Santhosh Kumar, D. Pamu, Ferroelectrics **516**, 173–184 (2017)
2. R.K. Bhuyan, T.S. Kumar, D. Goswami, A.R. James, A. Perumal, D. Pamu, Mater. Sci. Eng. B **178**, 471–476 (2013)
3. B.J. Li, S.Y. Wang, Y.H. Liao, Y.B. Chen, J. Ceram. Soc. Jpn. **122**, 955–958 (2014)
4. C.L. Huang, T.J. Yang, C.C. Huang, J. Am. Ceram. Soc. **92**, 119–124 (2009)
5. C.L. Huang, J.Y. Chen, J. Am. Ceram. Soc. **92**, 2237–2241 (2009)
6. C.L. Huang, C.E. Ho, Int. J. Appl. Ceram. Technol. **7**, E163–E169 (2010)
7. Y.B. Chen, J. Alloy Compd. **513**, 481–486 (2012)
8. R.K. Bhuyan, T.S. Kumar, D. Pamu, J.M. Renehan, M.V. Jacob, Mater. Express **4**, 349–357 (2014)
9. R.J. Cava, J. Mater. Chem. **11**, 54–62 (2001)
10. R.K. Bhuyan, T.S. Kumar, A.R. James, D. Pamu, Int. J. Appl. Ceram. Technol. **10**, E18–E24 (2013)
11. R.K. Bhuyan, T.S. Kumar, D. Goswami, A.R. James, D. Pamu, J. Electroceram. **31**, 48–54 (2013)
12. C.H. Lu, C.C. Tsai, Mater. Sci. Eng. B **55**, 95–101 (1985)
13. A. Belous, O. Ovchar, D. Durilin, M.M. Krzmanc, M. Valant, D. Suvorov, J. Am. Ceram. Soc. **89**, 3441–3445 (2006)
14. A. Wechsler, R.B. Von Dreele, Acta Crystallogr. B **45**, 542–549 (1989)
15. M. Kamruddin, P.K. Ajit Kumar, R. Nithya, A.K. Tyagi, B. Raj, Scr. Mater. **50**, 417–422 (2004)
16. H. Yang, Y. Hu, A. Tang, S. Jin, G. Qiu, J. Alloy Compd. **363**, 276–279 (2004)
17. K.T. Paul, S.K. Satpathy, I. Manna, K.K. Chakraborty, G.B. Nando, Nanoscale Res. Lett. **2**, 397–404 (2007)
18. L.B. Kong, J. Ma, W. Zhu, O.K. Tan, J. Alloy Compds. **322**, 290–297 (2001)
19. C. Suryanarayana, *Mechanical Alloying and Milling* (Marcel Dekker, New York, 2004)
20. G.K. Williamson, W.H. Hall, Acta Mater. **1**, 22–31 (1953)
21. J. Xu, G.S. Collins, L. Peng, M. Atzmon, Acta Mater. **47**, 1241–1253 (1999)
22. N. Obradovic, N. Labus, T. Sreckovic, M.M. Ristic, Mater. Sci. Forum **518**, 131–136 (2006)
23. H. Kominami, M. Tanaka, K. Hara, Y. Nakanishi, Y. Hatanaka, Phys. Status Solidi C **3**, 2758–2761 (2006)
24. A. Golubovic, M. Radovic, J. Serb. Chem. Soc. **76**, 1561–1566 (2011)
25. J. Stade, D. Hahn, R. Dittmann, J. Lumin. **8**, 308–317 (1974)
26. E.A.V. Ferri, J.C. Sczancoski, L.S. Cavalcante, E.C. Paris, J.W.M. Espinosa, A.T. de Figueiredo, P.S. Pizani, V.R. Mastelaro, J.A. Varela, E. Longo, Mater. Chem. Phys. **117**, 192–198 (2009)
27. R.K. Bhuyan, T.S. Kumar, A. Perumal, P. Saravanan, D. Pamu, J. Exp. Nanosci. **8**, 371–381 (2013)